

Non-Linear Elastic Response of Layered Structures, Alternating Pentamode Lattices and Confinement Plates

A. Amendola¹, F. Fraternali¹,

¹Department of Civil Engineering, University of Salerno, Via Giovanni Paolo II 132, 84084 Fisciano (SA), Italy. adaamendola1@unisa.it (A. Amendola), f.fraternali@unisa.it (F. Fraternali).

Keywords: Pentamode Metamaterials, Large Elastic Strains, Seismic Isolation, Impact Protection.

Abstract

We study the mechanical response under large elastic strains of pentamode layers confined between stiffening plates, and the potential use of such systems as novel seismic isolation and impact protection devices. We analyze pentamode materials that exhibit three soft deformation modes in the infinitesimal stretching regime that follow by the presence of perfectly hinged connections between the rods. The response of these metamaterials under large elastic strains is characterized by an elastic-stiffening effect in terms of the lateral force-displacement response, which increases in the presence of rigid connections and hard-device loading conditions, and decreases by increasing the number of layers. Our results lead us to conclude that the analyzed pentamode metamaterials can be effectively employed as novel, performance-based impact protection gear and seismic isolation devices by designing the lattice geometry, the stiffness properties of the joints, and the lamination scheme in a suitable manner and as a function of the operating conditions.

1. Introduction

In the last few years, mechanical and acoustic metamaterials have attracted the attention from different areas of research because of their unique behavior. Such smart materials are artificial structured lattices whose mechanical properties are mainly derived by their geometrical structure rather than their chemical composition (refer, e.g., to papers [1][2]). The class of “extremal materials” has been introduced in [3] to define materials that behave as extremely stiff in some mode of deformation and extremely soft in other modes. These are called uni-mode, bi-mode, tri-mode, quadra-mode and penta-mode materials, deriving from the number of the small mode of deformation they can achieve. This definition applies to a special class of mechanical metamaterials – composite materials, structural foams, cellular materials, etc. – which feature special mechanical properties. A specific category of extremal materials, called penta-mode meta-materials, have received particular attention in the literature. In particular, 3D printing techniques have been employed to manufacture such materials both at the macroscale [4][5] and microscale [6].

Pentamode metamaterials have five very small eigenvalues, meaning that they are very soft in five out of six principal directions of the elasticity tensor. This means that they show a very large bulk modulus (B), as compared to their shear modulus (G). The properties peculiar to pentamode metamaterials lead them to be suitable for many applications, such as transformation acoustics and elasto-mechanical cloak (refer, e.g., to [7]-[10] and the references therein). Their potential in different engineering fields is still only partially explored.

Whilst there are well-established measures to prevent the collapse of structures during seismic events such as earthquakes, these will not prevent a significant amount of damage being sustained in a seismic disturbance. Thus, there is now an impetus in the structural engineering field to further investigate methods that can reduce or even eliminate the damage that is typically sustained during these events (refer, e.g., to [11][12] and the references therein). One such method is seismic isolation,

which is receiving increased attention due to its effectiveness and ease of implementation on both existing and new structures. Seismic isolation has two fundamental concepts: to change the natural frequencies of the structure so they do not coincide with those frequencies of the seismic event, and the ability to dissipate a large amount of energy. The most popular seismic isolators in current use are elastomeric bearings, sliding bearings, and a combination of bearings with additional devices (e.g., with dissipative purposes) [11]-[16].

The ability of pentamode lattices to have both very soft and very stiff deformation modes suggests they are potentially suitable for use as seismic isolators [5], [17]-[19]. Unlike most other seismic isolators, where the response depends entirely on the properties of the materials used, the response of pentamode lattices depends mostly on their geometry. This is advantageous, as their response can be easily tuned by altering the geometry to control the vertical and horizontal stiffness for each application [5]. Previous studies have investigated the bending-dominated response of confined pentamode structures formed by alternating lattices with a face-centered-cubic (fcc) unit cell and stiffening plates (*fcc systems*) [5], [17]-[19]. Here we study a different kind of metamaterials, which use pentamode lattices whose unit cell consists of one half of the fcc cell (*sfcc systems*, cf. Sect. 2). By simulating the mechanical response of physical models of sfcc systems in the large elastic strain regime, we observe a stiffening effect in terms of the lateral force vs. lateral displacement response with increasing amplitude of lateral displacements, which becomes particularly relevant in the presence of rigid (moment-resisting) connections, and hard-device loading (Sect. 3). Such a geometrically nonlinear effect is accompanied by a softening response of vertical displacements under mixed-device loading, and becomes less effective by layering multiple sfcc layers, one over the other (cf. Sect. 3.2). It is worth noting that a similar hardening response is desired in triple friction pendulum bearings, with the aim of significantly increasing the stiffening of the device when the bearing reaches its ultimate displacement capacity [20][21]. Using a multi-layer design strategy, we are able to design laminated sfcc systems made of steel, which exhibit effective lateral stiffness approximatively equal to that of a commercial seismic isolator made of soft rubber-pads and thin steel shims. The analyzed sfcc pentamode bearings are tension-capable, i.e., can bear both compression and tension vertical loads during seismic excitations, due to the nonzero tensile strength of the rods forming the pentamode lattices (refer, e.g., to the recent paper [22], and references therein, for the technical relevance of tension-capable bearings). Sect. 4 summarizes the main results of the present study and suggests future research lines aimed at exploring the engineering potential of the pentamode metamaterials.

2. Physical models of sfcc pentamode metamaterials

The present section numerically investigates the elastic response of physical models of laminated pentamode metamaterials that show elementary modules of four rods meeting at a point confined between stiffening plates (sfcc systems, see Figure 1a). We employ steel bars grade S335JH, with Young modulus $E_o = 210$ GPa and yield strength $f_y = 355$ MPa [23][24], which can be connected to each other through the ball joint systems typically used in space grids [25]. We analyze lattices with 2×2 sfcc unit cells on the horizontal plane, each of which is composed of two elementary modules. The lattice constant a is set equal to 1200 mm, and the layer height is set equal to 600 mm. The stiffening plate edge length is equal to 2400 mm, and the rods are hollow circular tubes with length $l = 519.6$ mm.

We consider systems endowed with hinged, rigid or semi-rigid connections, in order to account for technical difficulties related to the manufacturing of perfectly hinged space grids; these problems are mainly due to the finite size of the bolts connecting the rods to the ball joints, and to friction effects at the nodes [25]. As we shall see, the analyzed systems may exhibit a marked stiffening response in the large elastic deformation regime (slope of the load-displacement curves markedly increasing with the lateral displacements). For that reason, and with the aim of preventing buckling and yielding

effects during the service behavior, our first results refer to lattices equipped with thick rods that feature 76.1 mm diameter and 5 mm wall thickness ($s = 1,116.84 \text{ mm}^2$) [23], which results in: $P_y = f_y s = 396.48 \text{ kN}$. On assuming perfectly hinged connections, the Eulerian critical load of the generic rods is: $P_{cr} = \pi^2 E_o I / \ell^2 = 5,444.23 \text{ kN}$; $I = 709,220.30 \text{ mm}^4$ denoting the moment of inertia of the cross-section. We will refer to such systems with the label 76SFCC. In Sect. 3.2, we will also examine lattices featuring relatively more slender rods, which have a 48.3 mm diameter and 5 mm wall thickness [23]; $s = 680.15 \text{ mm}^2$; $I = 161,527.42 \text{ mm}^4$; $P_y = 241.46 \text{ kN}$; $P_{cr} = \pi^2 E_o I / \ell^2 = 1,239.94 \text{ kN}$. We will refer to systems equipped with such rods as 48SFCC systems hereafter.

3. Large elastic deformations

We study the response of the models illustrated in the previous section under large elastic strains. We examine a displacement (or hard-device) loading condition, and a mixed-device, vertical force – lateral displacement loading condition on the top plate of the analyzed systems, always keeping the bottom plate at rest. The hard-device loading condition is applied to a monolayer system, while the mixed-device loading condition is applied both to a monolayer and multilayer system.

In the remainder, let F_x and F_z respectively denote the total forces acting on the top plate of the current system in the x - and z - directions. We use solid lines to indicate branches of the force-displacement curves such that all the members' cross sections are verified elastically under the action of the competent axial force (pre-axial-yielding branches: PAYB); and dashed lines to indicate branches in which such an axial yield check (AYC) is violated in one or more rods. We omit the change in the rods' cross-sectional properties, due to transverse deformation effects, when performing the above AYC. The study of the post-elastic behavior of the structures under examination is beyond the scope of the present work.

3.1 Hard-device loading

We apply a two-step displacement loading history on the top plate of a monolayer 76SFCC system, on assuming quasi-static loading conditions. First, we apply a downward uniform vertical displacement $d_z = d_z^0 = -1.478 \text{ mm}$ to the top plate. Next, we apply a uniform d_x – displacement ramp history to the top plate (in the positive x - direction), by keeping the above d_z displacement fixed. The elastic response of the system under consideration is analyzed in the large displacement regime, through the commercial finite element software Sap2000® version 18 [26][27] (Figure 1), and an in-house discrete element code . We employ two different finite element models: one featuring semi-rigid connections between the beam elements that describe the rods (SRC-FEM); and the other exhibiting rigid connections between such elements (RC-FEM). The SRC-FEM is obtained by introducing partial fixity rotational springs at the ends of each rod, and prescribing the following stiffness coefficients (both in torsion and bending) to each

$$K_\vartheta = \alpha E_o s \ell \quad (1)$$

α denoting a dimensionless parameter, and ϑ denoting the generic rotational degree of freedom (dof) at the end of the element [26]. Our simulation results assume $\alpha = 10^{-3}$, in order to allow the SRC-FEM to approximate a frame model with hinged/pinned connections. The RC-FEM instead assumes no releases of rotational dof at the extremities of each rod, and corresponds to prescribing $\alpha \rightarrow \infty$ in Eqn. (1). Finally, we employ a discrete element model (DEM) [28]-[29] that describes the junctions between the rods as point masses and the rods as linear springs, which implies a total release of the rotational dofs at the ends of each rod (perfectly hinged connections: $\alpha \rightarrow 0$) . In each of the above models, we model the stiffening plates as rigid elements, both in-plane and out-of-plane (combined diaphragm and plates constraints [26]). The employed FEMs make use of the Nonlinear Static Analysis available in Sap2000®, taking into account both P-delta and large-displacement effects [26]. It is worth remarking that sfcc systems equipped with pin joints are unstable under incremental lateral

displacements from the reference configuration [30]. For this reason, the response of the DEM equipped with hinged connections (HC-DEM) has been studied via the dynamic relaxation procedure presented in Ref. [31].

Table 1 shows the vertical stiffness coefficients $K_{v,0}$ recorded for the models under consideration in correspondence with the vertical preload phase (slope at the origin of the vertical force vs. vertical displacement curve). Such coefficients are similar to that of the HC-DE, which shows the stretching-dominated character of the response of the current models. For all the such models, we estimate a vertical preload $F_z^0 \approx -1.8$ MN under the prescribed value of d_z^0 , which corresponds to the vertical preload analyzed in the experimental tests on a commercial rubber bearing presented in Refs. [18]-[19] (the rubber bearing featured the following properties: diameter 0.85 m, height 0.35 m, 29 rubber layers of 7 mm each, 28 steel shims of 3.04 mm each, two terminal rubber layers of 31.8 mm each and covers, without lead plug data provided by Caltrans Testing Facility, University of California, San Diego).

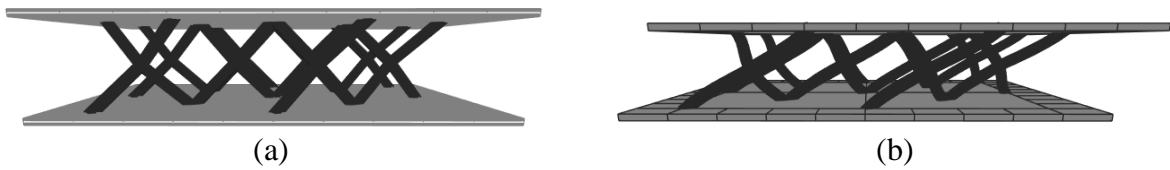


Figure 1. Finite element model of a monolayer 76SFCC system under hard-device loading: (a) reference configuration; (b) deformed shape under $d_x = 250$ mm (SRC-FEM).

Table 1. Vertical stiffness $K_{v,0}$ [kN/mm] of the analyzed monolayer 76SFCC systems.

HC-FEM	SRC-FEM	RC-FEM
1.204E+03	1.207E+03	1.208E+03

Figure 2 shows the force-displacement curves obtained for the HC-DEM, SRC-FEM and RC-FEM (see the inserts in Figure 2 for the behavior near the origin of such models). The deformed shape of the SRC-FEM under $d_x = 250$ mm is graphically illustrated in Figure 1b.

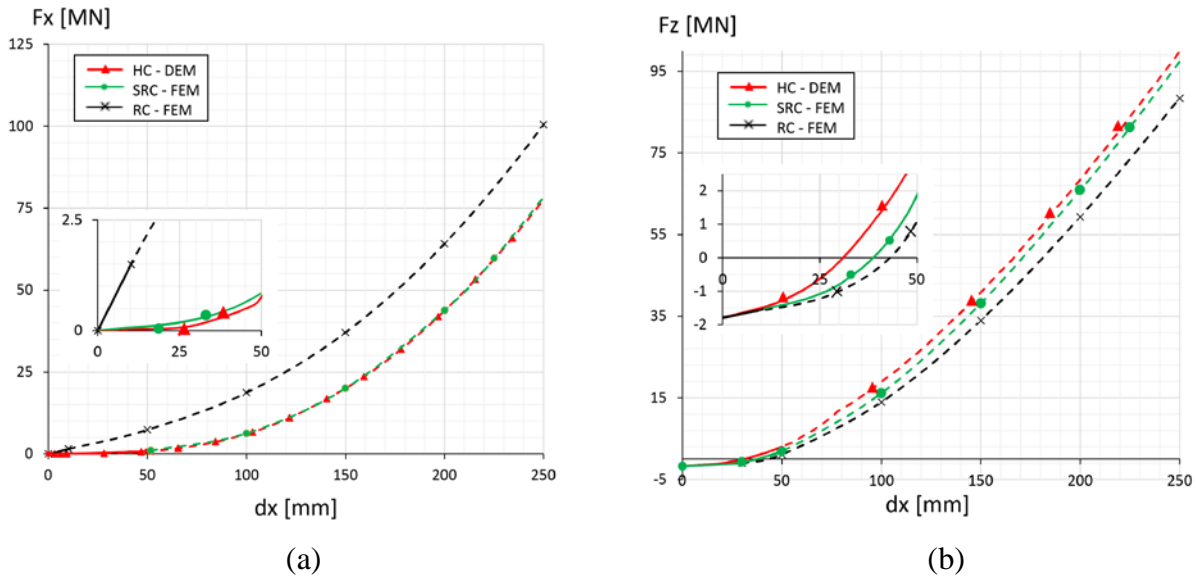


Figure 2. Force vs. displacement curves of monolayer 76SFCC systems under hard-device loading: (a) lateral force vs. lateral displacement; (b) vertical force vs. lateral displacement.

The results in Figure 2 highlight a marked stiffening (or hardening) character of the $F_x - d_x$ and $F_z - d_x$ curves exhibited by the analyzed models, for large or moderately large values of d_x . In the small displacement regime, we instead note that the $F_x - d_x$ curve of the HC-DEM features zero slope at the origin, which highlights that such a structure exhibits infinitesimal shear-type mechanisms from the reference configuration (cf. the insert in Figure 2a). The $F_x - d_x$ curve of the SRC-FEM instead shows a small positive slope at the origin. Finally, the $F_x - d_x$ curve of the RC-FEM features a markedly positive slope for $d_x = 0$. All the $F_z - d_x$ curves of the examined models start with $F_z \approx -1.8$ MN at $d_x = 0$, as a consequence of the vertical preload (see the insert in Figure 2b). It is interesting to observe that the F_z force rapidly assumes positive values (tensile forces on the top plate), as the lateral displacement d_x grows, in the current loading conditions ($d_z = d_z^0 = \text{const}$, while d_x grows). Of note here is that the analyzed systems are tension-capable [22], due to the nonzero tensile strength of the rods forming the pentamode lattices. The AYCs are violated already for $d_x \geq 10$ mm in the RC-FEM, as a consequence of the marked stiffening character of the force-displacement curve of such a system. The force-displacement curves of the SRC-FEM and HC-DEM are rather close together (stretching-dominated response), and the PAYBs of such curves extend up to $d_x \approx 50$ mm (Figure 2). It is worth observing that, while the $F_x - d_x$ curve of the RC-FEM is markedly stiffer than those of SRC-FEM and HC-DEM, the $F_z - d_x$ curves of the SRC-FEM and HC-DEM have slightly greater slope than the $F_z - d_x$ curve of the RC-FEM, (cf. Figure 2a and Figure 2b).

3.2 Mixed-device loading

Let us now study the response of a 76SFCC monolayer system under a fixed vertical load F_z , with increasing lateral displacements d_x of the top plate (mixed-device loading). We conduct such a study by focusing our attention on the SRC- and RC-FEMs described in the previous section, based on the consideration that perfectly hinged systems are not easily implemented in practice, especially when dealing with large displacements (due to unavoidable friction effects at the nodes). Figure 3 shows the lateral force vs. lateral displacement curves obtained for the SRC-FEM and the RC-FEM in correspondence with several values of the vertical load F_z . The results in Figure 3 highlight that the RC-FEM carries large horizontal forces and features a marked stiffening response under increasing lateral displacements, for any of the examined vertical loads, as we already observed in hard-device conditions. The PAYB of such a system extends up to $d_x \approx 50$ mm under zero vertical load, and $d_x \approx 35$ mm under $F_z = -1.8$ MN. The $F_x - d_x$ curves of the SRC-FEM instead feature a low-stiffness branch up $d_x \approx 400$ mm, which is followed by a markedly stiff branch ($d_x > 400$ mm). The PAYB of the SRC-FEM goes up to $d_x \approx 280$ mm under zero vertical load, and $d_x \approx 330$ mm under $F_z = -1.8$ MN.

The multi-layer 76SFCC and 48SFCC systems were examined, under the same mixed-device loading condition as above, assuming $F_z = -1.0$ MN as vertical preload (Figure 4). Table 2 shows the vertical stiffness coefficients $K_{v,0}$ obtained for the SRC- and RC-FEMs of such systems, which we will often denote by the short-hand notations SRC-76/48SFCC and RC-76/48SFCC, respectively. The $K_{v,0}$ coefficients of the models equipped with n_z layers are approximately equal to $1/n_z$ of those competing to the corresponding monolayer systems.

The $F_x - d_x$ curves of 76SFCC systems equipped with different numbers of layers are shown in Figure 5. In the two- and three-layer systems equipped with semi-rigid connections, we observe a significant reduction of the hardening effect found in the monolayer case. The PAYB of the RC-76SFCC systems switches from $d_x < 39$ mm in the monolayer case to $d_x < 68$ mm and $d_x < 91$ mm in two- and three-layer systems, respectively. Concerning the SRC-76SFCC systems, we observe that the PAYB of the monolayer case goes up to $d_x < 343$ mm, and that yielding does not occur at all in the two- and three-layer systems, up to $d_x = 500$ mm.

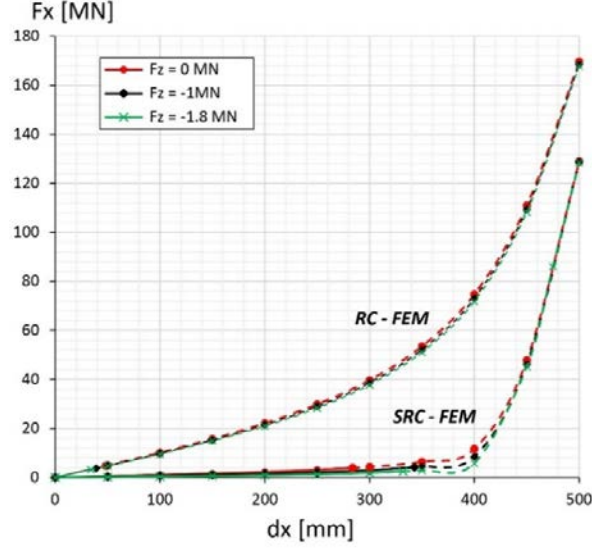


Figure 3. Lateral force vs. lateral displacement curves of RC- and SRC-FEMs of monolayer 76SFCC systems under mixed-device loading.

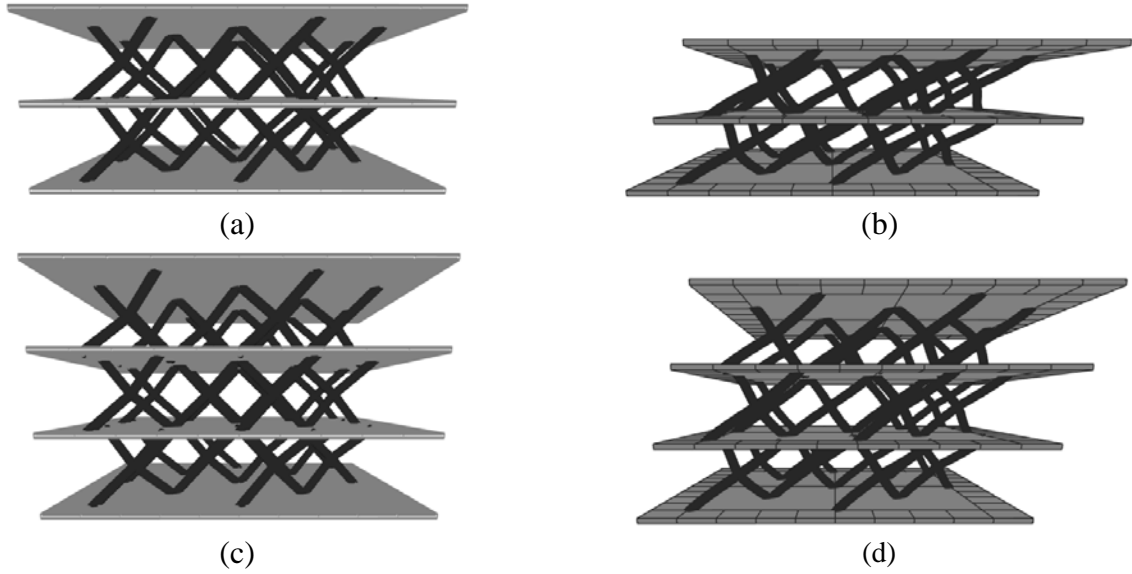


Figure 4. Illustrations of multilayer SRC-76SFCC finite element models. (a-b): Reference configuration (a) and deformed shape under $d_x = 500$ mm (b) of a two-layer system. (c-d): Reference configuration (c) and deformed shape under $d_x = 500$ mm (d) of a three-layer system.

Table 3 compares the effective (secant) stiffness $K_{h,eff}$ of mono- and multi-layer systems at the endpoints of the displacement ranges $d_x \in [0-250]$ mm and $d_x \in [0-500]$ mm. There is a marked abatement of $K_{h,eff}$ when passing from mono- to multi-layer systems. With reference to the loading interval $d_x \in [0-500]$ mm and the SRC-76SFCC models, we observe that the $K_{h,eff}$ of the systems with $n_z = 2$ and $n_z = 3$ are $\sim 1/74$ and $\sim 1/133$ of that exhibited by the monolayer system, respectively. In the same loading interval of the SRC-48SFCC models, the $K_{h,eff}$ of the systems with $n_z = 2$ and $n_z = 3$ are instead respectively $\sim 1/68$ and $\sim 1/81$ of the $K_{h,eff}$ corresponding to the case with $n_z = 1$. It is worth noting that such reductions are much larger than the analogous reductions of $K_{v,0}$ when passing from mono- to multi-layer systems (cf. Table 3 and Table 2).

We also observe that the $K_{h,eff}$ exhibited at $d_x = 500$ mm by the SRC models are of the same order of magnitude of the $K_{h,eff}$ recorded for a commercial rubber bearing in Refs. [18]-[19] ($K_{h,eff} \sim 1.5$ - 2.0 kN/mm; $K_{v,eff} \sim 700$ kN/mm).

Table 2. Vertical stiffness $K_{v,0}$ [kN/mm] of the analyzed systems under mixed-device loading, for varying numbers of layers n_z .

<i>type</i>	n_z	SRC-FEM	RC-FEM
76SFCC	1	1207.01	1208.04
76SFCC	2	610.70	621.10
76SFCC	3	417.52	420.50
48SFCC	1	736.55	747.60
48SFCC	2	368.14	373.66
48SFCC	3	245.27	248.95

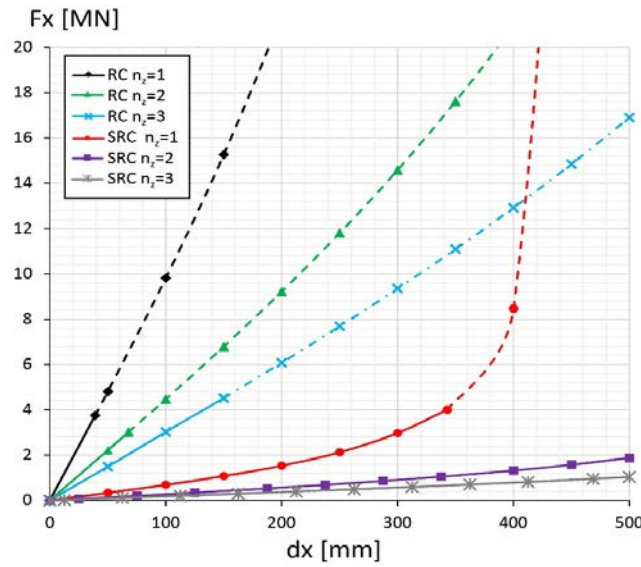


Figure 5. Lateral force vs. lateral displacement curves of 76SFCC systems for varying numbers of layers n_z , under mixed-device loading.

Table 3. Effective horizontal stiffness $K_{h,eff}$ of the analyzed multilayer systems.

<i>type</i>	n_z	RC - FEM		SRC - FEM	
		$K_{h,eff}$ [kN/mm]		$K_{h,eff}$ [kN/mm]	
		[0-250] mm	[0-500] mm	[0-250] mm	[0-500] mm
76SFCC	1	115.97	337.15	8.49	257.24
76SFCC	2	47.20	57.83	2.88	3.74
76SFCC	3	30.72	33.78	1.85	2.07
48SFCC	1	26.81	182.65	5.21	167.95
48SFCC	2	10.35	13.74	1.76	2.47
48SFCC	3	6.77	7.62	1.86	2.07

Figure 6 (a) compares the lateral force vs. lateral displacement curves of SRC-76SFCC and SRC-48SFCC systems, and demonstrates that the PAYB of the monolayer 76SFCC system ($d_x < 343$ mm) is slightly wider than that of the monolayer 48SFCC system ($d_x < 302$ mm). The F_x vs. d_x curves of the 76SFCC systems are stiffer than those of the 48SFCC systems, in the cases with $n_z = 1$ and $n_z = 2$. In the three-layer case, 76SFCC and 48SFCC systems instead feature a similar F_x vs. d_x response, as confirmed by the results given in Figure 6 (a) and Table 3. Figure 6 (b) shows the vertical displacement vs. lateral displacement curves of the SRC-76SFCC systems with different numbers of layers (displacements of the top-most layer). Snapshots of the deformed configurations of single- and two-layer systems are provided in Figure 7, in correspondence with selected values of the top-plate displacement d_x . The vertical displacements of the monolayer system are markedly larger than those exhibited by multilayer systems. The extremely large vertical displacements of the system with $n_z = 1$ would nearly reduce to zero the system height ($d_z = 525$ mm at $d_x = 500$ mm, cf. panel (i) of Figure 7). It is worth noting, however, that the dashed branch of the d_z vs. d_x curve for $n_z = 1$ is just theoretical, since the monolayer 76SFCC system would actually experience plastic deformations for $d_x > 343$ mm, instead of a purely elastic response (post-buckling branch). As we already observed, the maximum vertical displacement markedly reduces in magnitude by increasing the number of layers. The system with $n_z = 2$ indeed exhibits $d_z = 239$ mm for $d_x = 500$ mm, while the system with $n_z = 3$ exhibits $d_z = 153$ mm, always at $d_x = 500$ mm.

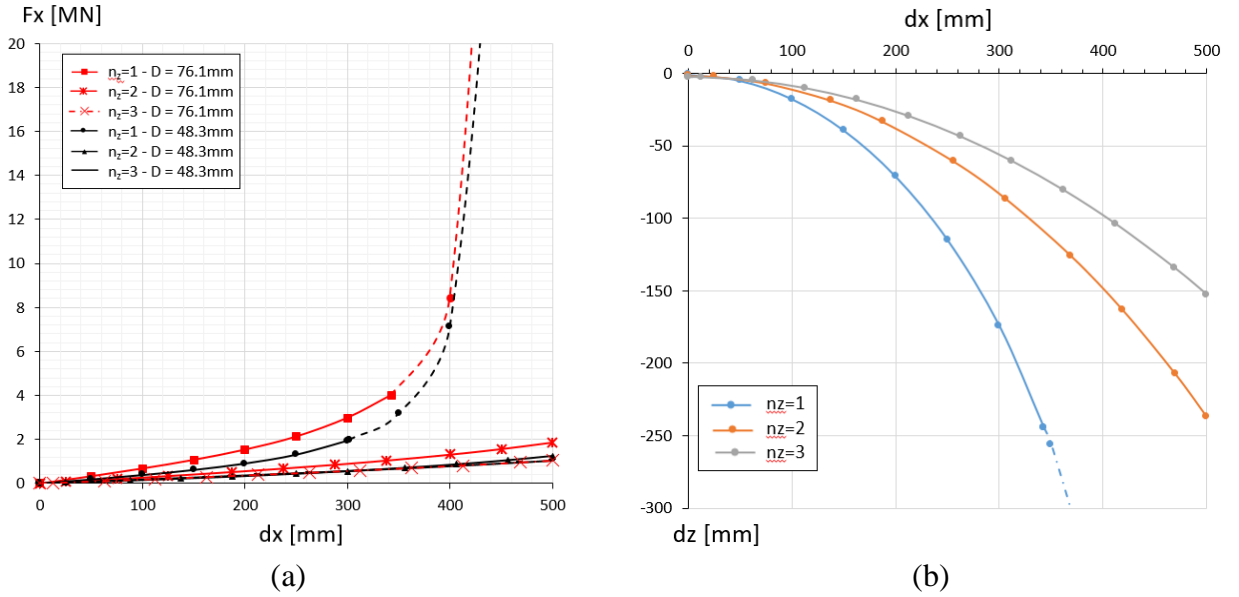


Figure 6. (a) Lateral force vs. lateral displacement curves of SRC-76SFCC and SRC-48SFCC systems with different numbers of layers. (b) Vertical displacement vs. lateral displacement curves of 76SFCC systems showing different numbers of layers.

We end by commenting on the distributions of the forces carried by the systems illustrated in Figure 7. Our results indicate that the rods of both single- and two-layer systems carry almost uniform distributions of compressive axial forces in correspondence with the vertical preload phase (cf. panels (a)-(b) of Figure 7). The compressive forces carried by the rods inclined towards the direction of the applied lateral displacement (i.e., towards the positive x -axis) progressively turn into tensile forces, for increasing values of d_x (see panels (c)-(j) of Figure 7 for the deformed shapes corresponding to $d_x > 0$).

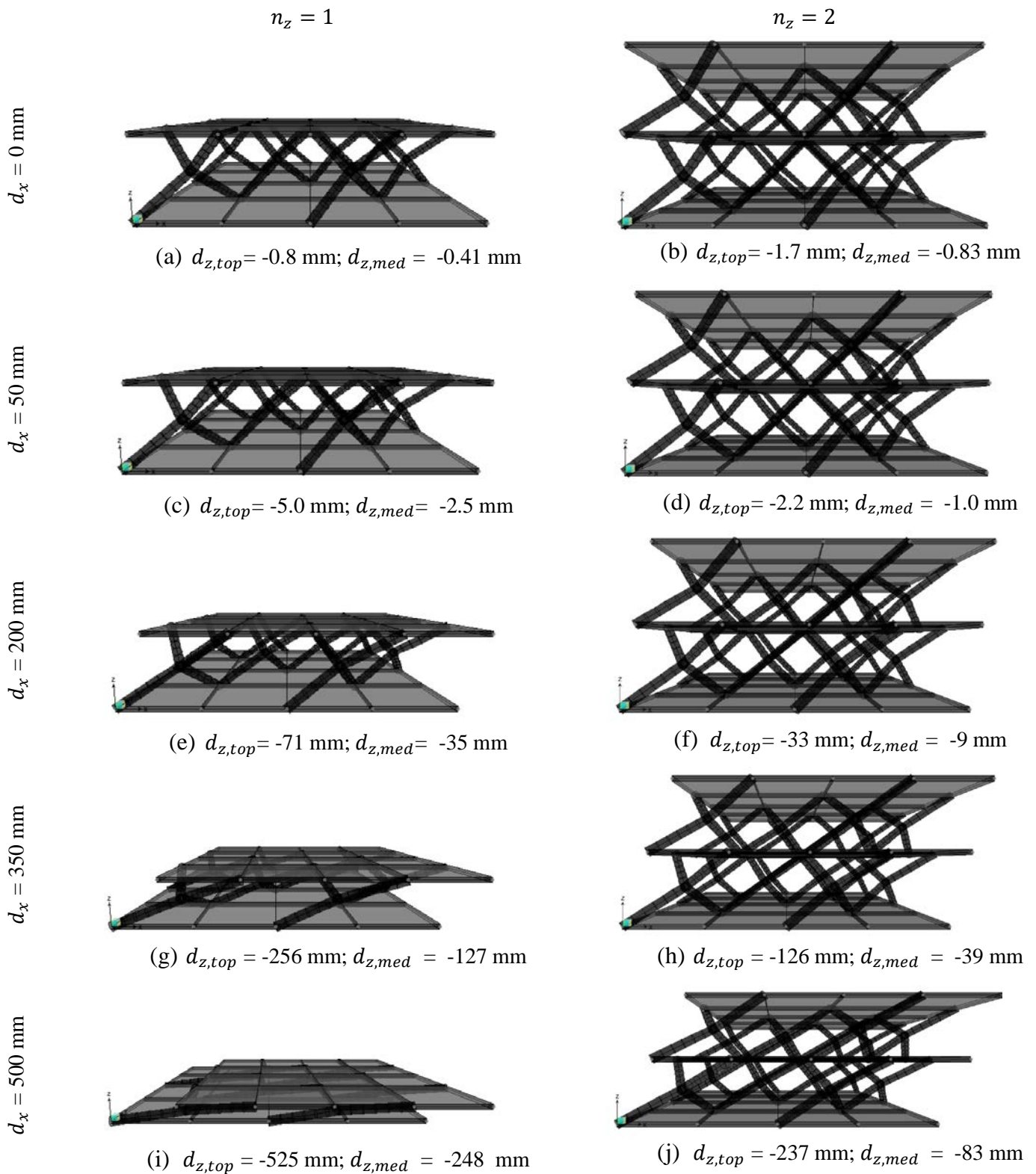


Figure 7. Deformed configurations of SRC-FEMs relative to mono- and bi-layer 76SFCC systems, for different values of the top-plate lateral displacement d_x ($d_{z,top}$: vertical displacement of the top plate; $d_{z,med}$: vertical displacement of the mid-horizontal layer).

The configuration under $d_x = 500$ mm of the single-layer system shows all the rods under tensile forces and the top plate almost collapsed onto the bottom plate. As we already noted, such a configuration is only theoretical, since it contemplates very large tensile forces in the rods inclined towards the positive x - axis, which are markedly greater than the yielding force P_y (cf. panel (i) of Figure 7). Instead, the two-layer system carries much lower axial forces than the single-layer system. In such a system, tensile forces act in the rods inclined towards the $+x$ - axis, and compressive forces act in the rods inclined towards the $-x$ - axis. Both forces always result in $P < P_y$, up to $d_x = 500$ mm. With reference to such a system, we find that the shear forces carried by the rods grow with the lateral displacement d_x , featuring maximum values approximatively equal to 0.07, 0.19, 0.39, 0.54, 0.66 and 0.74 of the maximum axial forces, for d_x respectively equal to 50 mm, 100 mm, 200 mm, 300 mm, 400 mm and 500 mm. The bending moments approximatively exhibit values equal in magnitude but opposite in sign at the ends of each rod, with extreme values circa equal to one half of the competent shear force multiplied by the rod length. Finally, the twisting moments carried by the rods are approximatively one order of magnitude smaller than the bending moments. The above results provide evidence of a transition from a stretching-dominated response to a coupled stretching-bending regime of the systems equipped with semi-rigid connections, for growing values of the lateral displacements.

4. Concluding remarks

We have studied the nonlinear elastic response of novel metamaterials obtained by stiffening sfcc pentamode layers with confinement plates. We observed that the infinitesimal mechanisms exhibited by the examined systems in the small displacement regime switch to a stiffening lateral force vs. lateral displacement response under large displacements (Sect. 3). Such geometrically nonlinear behavior, which is also found in different lattice structures [32]-[34] and triple friction pendulum bearings [20][21], can be finely adjusted by playing with the bending rigidity of the nodes and the number of layers (cf. Sect. 3.2).

The results of the present study allowed us to extend recent findings on the bending-dominated response of confined pentamode lattices [5], [17]-[19] to the case of the stretching-dominated or coupled stretching-bending response of sfcc pentamode metamaterials equipped with hinged or semi-rigid connections. We were able to design sfcc multi-layer systems entirely made of steel (using steel both for the stiffening plates and the pentamode lattices), which exhibit effective lateral stiffness approximatively equal to that of a commercial seismic isolator made of soft rubber-pads and thin steel shims (Sect. 3.2). Their use as stop-band materials for shear waves [7]-[9] within novel impact protection gears awaits attention.

We may conclude that pentamode bearings offer several advantages over other available structural bearings [11]-[14], which mainly follow from the fact that such systems can be easily designed to behave as tension-capable and performance-based systems, and because their mechanical properties are driven largely by the geometry of the lattice microstructure, rather than the chemical composition of the material (i.e. such systems behave as mechanical metamaterials). It is worth noting that it is possible to play with the lattice microstructure in order to achieve the desired combination of shear and compression response (cf. Sect. 3 and Refs. [5], [17]-[19]). Moreover, the choice of the material offers additional design opportunities, both in terms of the elastic response, and for what concerns the energy dissipation properties of the system. We have also observed that it is possible to design laminated structures that feature multiple pentamode layers equipped with different materials and properties, while in laminated rubber bearings the only lamination variable relative to the soft layers consists of the use of natural or synthetic rubber [5]. Finally, pentamode bearings can be manufactured on employing rapid prototyping techniques that make use of single or multiple materials (metals, polymers, etc.) [4]-[6], and space grid technologies employing ball-joint systems [25].

Future extension of the present research will regard experimental testing of real-scale physical models of pentamode bearings [35], the modeling of plastic and fracture damage in the rods of pentamode bearings under significant strains [36]-[38], and discrete-to-continuum approaches to the mechanics of confined multilayered structures [39]-[41]. Peculiar features of the examined systems, which suggest additional directions for future work, include their increasing lateral rigidity and vertical deformability in the large lateral displacement regime (cf. Sect. 3.2). We recommend that future studies undertake detailed investigations of such geometrically nonlinear effects, with areas of focus including the examination of systems with variable numbers of layers, the inclusion of dissipative and stiffening members within the pentamode layers, and the use of lateral confinement/pre-stress techniques.

Acknowledgements

A. Amendola gratefully acknowledges financial support from the Ph.D. School in Civil Engineering at the University of Salerno. The authors wish to thank Gerardo Carpentieri, Mariella De Piano and Raffaele Miranda, from the Department of Civil Engineering of the University of Salerno, and Pasquale Gagliardi, from Vestrut Engineering s.r.l. (<http://www.vestrut.it/en/>), for their helpful assistance with the numerical results and the design of physical models of sfcc systems. The authors would also like to acknowledge the valuable assistance of Dr. Gianmario Benzoni (Department of Structural Engineering, University of California, San Diego) with the seismic engineering aspects of the present research.

References

- [1] Lu, M.H., Feng, L., Chen, Y.F., 2009. Phononic crystals and acoustic metamaterials. *Mater. Today* 12, 34-42.
- [2] Maldovan, M., 2013. Sound and heat revolution in phononics. *Nature* 503, 209-217.
- [3] Milton, G.W., Cherkaev, A.V., 1995. Which Elasticity Tensors are Realizable? *J. Eng. Mater.-T* 117(4), 483-493.
- [4] Schittny, M., Bückmann, T., Kadic, M., Wegener, M., 2013. Elastic measurements on macroscopic three-dimensional pentamode metamaterials. *Appl. Phys. Lett.* 103.
- [5] Amendola, A., Smith, C.J., Goodall, R., Auricchio, F., Feo, L., Benzoni, G., Fraternali, F., 2016. Experimental response of additively manufactured metallic pentamode materials confined between stiffening plates. *Compos. Struct.* 142, 254-262.
- [6] Kadic, M., Bückmann, T., Stenger, N., Thiel, M., Wegener, M., 2012. On the practicability of pentamode mechanical metamaterials. *Appl. Phys. Lett.* 100.
- [7] Martin, A., Kadic, M., Schittny, R., Bückmann, T., Wegener, M., 2010. Phonon band structures of three-dimensional pentamode metamaterials. *Phys. Rev. B* 86, 155116.
- [8] Huang, Y., Lu, X., Liang, G., Xu, Z., 2016. Pentamodal property and acoustic band gaps of pentamode metamaterials with different cross-section shapes. *Phys. Lett. A* 380(13), 1334-1338.
- [9] Bückmann, T., Thiel, M., Kadic, M., Schittny, R., Wegener, M., 2014. An elastomechanical unfeelability cloak made of pentamode metamaterials. *Nat. Comm.* 5, 4130.
- [10] Chen, Y., Liu, X., Hu, G., 2015. Latticed pentamode acoustic cloak. *Scientific Reports* 5:15745.
- [11] Skinner, R.I., Robinson, W.H., Mcverry, G.H., 1993. *An introduction to seismic isolation*. Wiley.
- [12] Kelly, J.M., 1993. *Earthquake-resistant design with rubber*. London: Springer-Verlag.

- [13] Benzoni, G., Casarotti, C., 2009. Effects of Vertical Load, strain rate and cycling on the response of lead-rubber seismic isolators. *J. Earthquake Eng.* 13(3), 293-312.
- [14] Higashino, M., Hamaguchi, H., Minewaki, S., Aizawa, S., 2003. Basic characteristics and durability of low-friction sliding bearings for base isolation. *Earthquake Eng. Eng. Seismolog.* 4(1), 95-105.
- [15] Warn, G. P., Whittaker, A. S., Constantinou, M.C., 2007. Vertical stiffness of elastomeric and lead-rubber seismic isolation bearings. *J. Struct. Eng.-ASCE* 133 (9), 1227-1236.
- [16] European Committee for Standardization. Anti-seismic devices, EN 15129. Brussels, Belgium, 2009.
- [17] Amendola, A., Carpentieri, G., Feo, L., Fraternali, F., 2016. Bending dominated response of layered mechanical metamaterials alternating pentamode lattices and confinement plates. *Compos. Struct.* 151, 71-77.
- [18] Fraternali, F., Carpentieri, G., Montuori, R., Amendola, A., Benzoni, G., 2015. On the use of mechanical metamaterials for innovative seismic isolation systems. In: *Compdyn 2015 - 5th Ecomas thematic conference on computational methods*. In: *Structural Dynamics and Earthquake Engineering*, 349-358.
- [19] Fabbrocino, F., Amendola, A., Benzoni, G., Fraternali, F., 2016. Seismic application of pentamode lattices. *Ingegneria Sismica/International J. Earthquake Eng.* 1-2, 62-71.
- [20] Becker, T.C., Mahin, S.A., 2012. Experimental and analytical study of the bi-directional behavior of the triple friction pendulum isolator. *Earthquake Eng. Struct. Dyn.* 41, 355–373.
- [21] Fenz, D.M., Constantinou, M.C., 2008. Modeling triple friction pendulum bearings for response-history analysis. *Earthq. Spectra* 24, 1011-1028.
- [22] Zhou, Z., Wong, J., Mahin, S., 2016. Potentiality of using vertical and three-dimensional isolation systems in nuclear structures, *Nucl. Eng. Technol*, Online First, DOI: <http://dx.doi.org/10.1016/j.net.2016.03.005>
- [23] EN 10210-2:2006, Hot finished structural hollow sections of non-alloy and fine grain steels - Part 2: Tolerances, dimensions and sectional properties.
- [24] EN 1993-1-1:2005. Eurocode 3: Design of Steel Structures – Part 1-1: General Rules and Rules for Buildings, European Committee for Standardization, May 2005.
- [25] J. Chilton, *Space Grid Structures*, Oxford, UK, 2000.
- [26] CSI, Computers & Structures, Inc. Analysis reference manual for SAP2000® version 18. Berkeley, California, USA, June 2015.
- [27] CSI, Computers & Structures, Inc. Steel Frame Design Manual for SAP2000® version 18. Berkeley, California, USA, September 2015.
- [28] Leonard, A., Fraternali, F., Daraio, C., 2013. Directional wave propagation in a highly nonlinear square packing of spheres. *Exp. Mech.* 53(3), 327-337.
- [29] Daraio, C., Ngo, D., Nesterenko, V.F., Fraternali, F., 2010. Highly nonlinear pulse splitting and recombination in a two dimensional granular network. *Phys. Rev. E* 82, 036603.
- [30] Norris, A.N., 2014. Mechanics of elastic networks. *Proc. R. Soc. A* 470, 20140522.
- [31] Fraternali, F., Blesgen, T., Amendola, A., Daraio, C., 2011. Multiscale Mass-Spring Models of Carbon Nanotube Foams. *J. Mech. Phys. Solids.* 59, 89-102.
- [32] Amendola, A., Carpentieri, G., De Oliveira, M., Skelton, R.E., Fraternali, F., 2014. Experimental investigation of the softening-stiffening response of tensegrity prisms under compressive loading. *Compos. Struct.* 117, 234-243.

- [33] Fraternali, F., Carpentieri, G., Amendola, A., 2015. On the mechanical modeling of the extreme softening/stiffening response of axially loaded tensegrity prisms. *J. Mech. Phys. Solids* 74, 136-157.
- [34] Fraternali, F., Carpentieri, G., Amendola, A., Skelton, R.E., Nesterenko, V.F., 2014. Multiscale tunability of solitary wave dynamics in tensegrity metamaterials. *Appl. Phys. Lett.* 105, 201903.
- [35] Modano, M., Fabbrocino, F., Gesualdo, A., Matrone, G., Farina, I., Fraternali, F., 2015. On the forced vibration test by vibrodyne. *COMPADYN 2015 - 5th ECCOMAS Thematic Conference on Computational Methods in Structural Dynamics and Earthquake Engineering*, 209-217.
- [36] Fraternali, F., 2007. Free Discontinuity Finite element models in two-dimensions for in-plane crack problems. *Theor. Appl. Fract. Mec.* 47, 274-282.
- [37] Schmidt, B., Fraternali, F., Ortiz, M., 2009. Eigenfracture: An Eigendeformation Approach to Variational Fracture. *Multiscale Model. Sim.* 7(3), 1237-1266.
- [38] Elsayed, T., Mota, A., Fraternali, F., Ortiz, M. A., 2008. Variational Constitutive Model for Soft Biological Tissues, *J. Biomech.* 41(7), 1458-1466.
- [39] Fraternali, F., Lorenz, C.D, Marcelli, G., 2012. On the estimation of the curvatures and bending rigidity of membrane networks via a local maximum-entropy approach. *J. Comput. Phys.* 231, 528-540.
- [40] Fraternali, F., Marcelli, G., 2012. A multiscale approach to the elastic moduli of biomembrane networks. *Biomech. Model. Mechan.* 11(7), 1097-1108.
- [41] Schmidt, B., Fraternali, F., 2012. Universal formulae for the limiting elastic energy of membrane networks. *J. Mech. Phys. Solids* 60, 172-180.